Article

Estimation of Forest Canopy Fuel Moisture Content in Dali Prefecture by Combining Vegetation Indices and Canopy Radiative Transfer Models from MODIS Data

Kun Yang [1,2], Bo-Hui Tang [1,2,3,*], Wei Fu [1,2], Wei Zhou [1,2], Zhitao Fu [1,2] and Dong Fan [1,2]

1 Faculty of Land Resources Engineering, Kunming University of Science and Technology, Kunming 650093, China; yangkun05@stu.kust.edu.cn (K.Y.); fuwei@stu.kust.edu.cn (W.F.); 20212201152@stu.kust.edu.cn (W.Z.); zhitaofu@kust.edu.cn (Z.F.); dongfan@kust.edu.cn (D.F.)
2 Key Laboratory of Plateau Remote Sensing, Department of Education of Yunnan Province, Kunming 650093, China
3 State Key Laboratory of Resources and Environmental Information System, Institute of Geographic Sciences and Natural Resources Research, Chinese Academy of Sciences, Beijing 100101, China
* Correspondence: tangbh@kust.edu.cn

Abstract: Forest canopy fuel moisture content (FMC) is a critical factor in assessing the vulnerability of a specific area to forest fires. The conventional FMC estimation method, which relies on look-up tables and loss functions, cannot to elucidate the relationship between FMC and simulated data from look-up tables. This study proposes a novel approach for estimating FMC by combining enhanced vegetation index (EVI) and normalized difference moisture index (NDMI). The method employs the PROSAIL + PROGeoSAIL two-layer coupled radiation transfer model to simulate the vegetation index, the water index, and the FMC value, targeting the prevalent double-layer structure in the study area's vegetation distribution. Additionally, a look-up table is constructed through numerical analysis to investigate the relationships among vegetation indices, water indices, and FMC. The results reveal that the polynomial equations incorporating vegetation and water indices as independent variables exhibit a strong correlation with FMC. Utilizing the EVI–NDMI joint FMC estimation method enables the direct estimation of FMC. The collected samples from Dali were compared with the estimated values, revealing that the proposed method exhibits superior accuracy (R2 = 0.79) in comparison with conventional FMC estimation methods. In addition, we applied this method to estimate the FMC in the Chongqing region one week before the 2022 forest fire event, revealing a significant decreasing trend in regional FMC leading up to the fire outbreak, highlighting its effectiveness in facilitating pre-disaster warnings.

Keywords: forest canopy fuel moisture content; PROSAIL; PROGeoSAIL; enhanced vegetation index; normalized difference moisture index

1. Introduction

Forest fires pose significant and formidable challenges in today's world. Countries across temperate, subtropical, and tropical regions are grappling with the menace of forest fires due to the escalating impacts of global warming and heightened weather extremes [1,2]. The accurate and efficient early warning and monitoring of forest fires pose a critical issue that governments must presently confront [3].

Forest fire events are influenced by multiple interacting factors. According to Pyne's wildfire triangle model [4], the occurrence of wildfires is primarily determined by climate, topography, and fuels. Currently, early-warning methods for forest fires can be classified into three main categories: fire weather forecasts, forest fire occurrence forecasts, and forest fire behavior forecasts. The advancement of satellite remote sensing and internet big data technology has facilitated the integration of weather conditions, combustible materials, and

fire sources, leading to a mainstream approach known as forest fire forecasting, which aims to predict the risk of forest fires [5].

Due to the complexity of the forest ecosystem, various factors in the wildfire triangle model interact with each other within the natural environment [6]. This phenomenon means that the influence of other factors on the relevant parameters of many forest areas cannot be ignored in forest fire forecasting [7,8]. Undoubtedly, this complexity and difficulty increase the challenges associated with forest fire forecasting.

Forest canopy fuel moisture content (FMC) acts as an important indicator reflecting the dryness or wetness levels of wild vegetation while also significantly contributing to evaluating susceptibility to forest fires. Previous research has demonstrated that when the FMC falls below 100%, there is a significant increase in forest fire occurrence probability [9]. The sensitivity of FMC to weather conditions and internal vegetation dynamics makes it one of an exemplary factor for forecasting forest fires among numerous others [10]. Consequently, the precise retrieval of FMC through remote sensing assumes paramount importance as a fundamental step in evaluating forest fire risk.

Traditional methods for measuring FMC suffer from several limitations, such as their high demand for manpower and resources. Consequently, they are generally inefficient and unable to comprehensively cover vast forest areas. However, satellite remote sensing technology offers a solution by providing real-time observations across extensive regions [11]. This technological advancement overcomes the inefficiencies associated with traditional physical parameter measurement methods and facilitates the prolonged monitoring of FMC in large forest regions [12,13].

The most direct approach to quantitatively inverting FMC by using remote sensing is to establish a correlation between vegetation canopy spectra and FMC. Some researchers have explored this relationship through spectroscopic and spectral analyses, aiming to construct empirical models that link spectral indices to FMC. These models rely on spectral measurements of vegetation and corresponding field data on FMC [14,15]. However, the construction of such empirical models requires a substantial number of field observations and data samples. Additionally, these empirical models are area-specific in nature. As a result, many researchers are inclined towards utilizing physical models for the quantitative retrieval of FMC. Numerous studies have indicated that FMC can be approximated by two parameters within the PROSPECT model [16] of leaf reflectance: equivalent water thickness (EWT) and dry matter content (DMC). Therefore, radiative transfer models can be employed to simulate vegetation spectral reflectance and estimate FMC [17]. Commonly used models include the two-dimensional PROSAIL model [18], the Liberty model [19], the GEOSAIL model [20], and the three-dimensional DART model [21–23]. The merit and demerit of the FMC estimation methods described above are presented in Table 1.

Table 1. Comparison of FMC estimation methods.

Model Type	Model	Merit	Demerit
Empirical model	Spectral model	High accuracy in estimating FMC.	Needs a large number of measured data; existence of regional limitations.
Physical model	PROSAIL	Can be approximated by estimating EWT and DMC; high accuracy in estimating FMC for uniformly distributed vegetation.	Only suitable for vegetation with uniform canopy distribution; has hot spot effect.
	Liberty	Suitable for coniferous forests.	Lack of dry matter weight parameter; can only be approximated by other parameters.
	GEOSAIL	Suitable for reflectance simulation of heterogeneous canopy.	Has hot spot effect.
	DART	Three-dimensional model; the light transmission process of forest canopy can be well restored.	Large amount of calculation.

The PROSAIL model, which integrates the leaf optical model PROSPECT with the canopy radiative transfer model SAIL, is extensively employed for biophysical and chemical parameter retrieval, as well as spectral simulation. It has demonstrated high accuracy in estimating FMC for uniformly distributed vegetation. Numerous researchers have utilized the PROSAIL model to estimate FMC in grasslands and crops [24]. Previous studies have indicated significant correlations between various indices, such as NDVI, EVI, NDWI, and NDMI, and FMC, and regression models incorporating these indices along with measured FMC data achieve remarkable accuracy [25]. However, when dealing with forests characterized by tall and irregular canopy structures along with complex understory environments, the selection of suitable models for FMC estimation becomes more diverse [26,27].

Further research and analysis have shown good agreement between vegetation parameters derived from physical models or look-up table-based methods and measured data [28]. Multiple-model analyses and accuracy evaluations of inverse canopy FMC estimation further revealed that the PROGEOSAIL model outperformed the Liberty model for sparse broadleaf and mixed conifer forests [29,30].

In response to the complex forest structure, improvements are being made to radiative transfer models. For the prevalent "tall trees + low vegetation" double-layered forest structures, some scholars have proposed combining the PROSAIL model with the PROGEOSAIL model to construct a look-up table approach, approximating FMC through a loss function [31]. While estimation of FMC based on physical models enhances applicability compared with empirical models, the presence of loss functions in the look-up table method creates an error between estimated and real values of FMC.

The objective of this research is to investigate the correlation between vegetation index/water index and FMC by examining their numerical relationship to develop a model for estimating FMC. Section 2 provides an overview of the study area and data utilized in this work, and the method of combining vegetation indices and canopy radiative transfer models to estimate FMC is presented. The results are shown in Section 3, followed by a discussion in Section 4. Finally, the conclusions are drawn in Section 5.

2. Materials and Methods

2.1. Materials

2.1.1. Study Area

The study area is situated in Dali Bai Autonomous Prefecture, Yunnan Province, China, at the confluence of the western Yunnan Central Plateau and the southern end of the Hengduan Mountains, covering a core area of 170 square kilometers with an average elevation of 2000 m (Figure 1). Influenced by the subtropical monsoonal climate pattern at low latitudes, the study area exhibits an annual rainfall distribution characterized by increases during summer and autumn and reductions during winter and spring. The rainy season spans from May to October, contributing to approximately 83% of the annual rainfall. Conversely, the dry season occurs from November to April, and accounts for only 17% of the annual rainfall. Dry weather conditions make forest fires likely to occur during this period. Additionally, the significant topographic relief in the area poses challenges for local fire services in controlling hill fires.
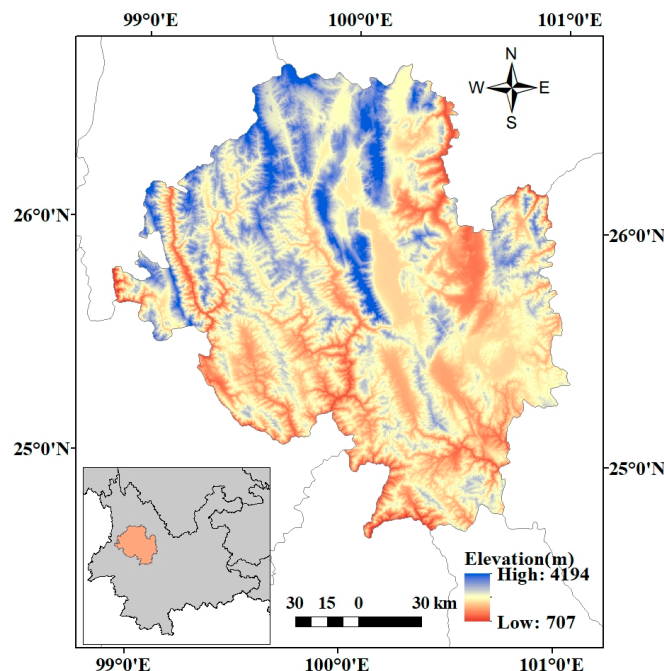
Figure 1. Elevation of the study area.

2.1.2. MODIS Satellite Data

MODIS is a medium-resolution imaging spectrometer deployed on the Terra and Aqua satellites and serves as a pivotal instrument in the US Earth Observation System (EOS) program for monitoring global biological and physical processes. Terra is the morning star, as it passes the equator from north to south at about 10:30 local time, and can acquire up to four transit orbits daily. Aqua is the afternoon star, as it passes the equator from south to north at about 13:30 local time. These two satellites collaborate harmoniously to repetitively observe the entire Earth's surface every 1–2 days, yielding a comprehensive dataset comprising 36 bands of data. For this study, we utilized MOD09GA daily 500 m surface reflectance data generated by MODIS from Terra (https://ladsweb.modaps.eosdis. nasa.gov/ (accessed on 1 April 2023)). This Level 2 product offers valuable insights into reflectance across bands 1–7, along with quality assessment ratings, observation ranges and counts, as well as information regarding scan values at a resolution of 250 m. For our analysis, we focused primarily on bands 01 (RED), 02 (NIR), 03 (BLUE), and 07 (SWIR) of the MOD09GA product.

2.1.3. Field Data

A predetermined number of quadrats were planned within this study area, and field sampling was conducted to collect vegetation canopy leaves. The quadrat was consistent with the spatial resolution of MODIS satellite imagery (500 m × 500 m). The selection of clear sky conditions and the maintenance of a specific distance between samples were prioritized during the planning stage. In this study, a total of 11 quadrats were designed in the Cangshan area. The central coordinates of quadrats are shown in Table 2. The spatial distribution of quadrats within the study area is illustrated in Figure 2.

The field samples were collected as follows: Firstly, the sample square number, the coordinates of the center of the sample square (latitude, longitude, and elevation), and the surrounding environment were recorded. Then, within each sample square, 5–10 canopy foliage samples were collected in a natural environment. The coordinates of the current sample point and the sample trees were also recorded and photographed. In each sample plot, 5–8 randomly selected adult leaves of uniform size were collected. Finally, the vegetation samples were sealed in bags, and relevant information was recorded on the bag using a marker. The samples were labeled with a unique number following the format

"A-B", where A represents the quadrat number and B represents the sample number within that particular quadrat. The collected vegetation samples were brought back to the laboratory for weighing purposes, and the fresh weight measurements were first obtained, followed by drying at a constant temperature of 65 °C for 24 h before obtaining dry weights. These two weight measurements were then utilized to calculate FMC as follows:

$$\text{FMC} = \frac{W_h - W_d}{W_d} \times 100\%, \tag{1}$$

where W_h is the fresh weight of the leaf sample and W_d is the dry weight of the leaf sample.

Table 2. Details of the ground sampling sites.

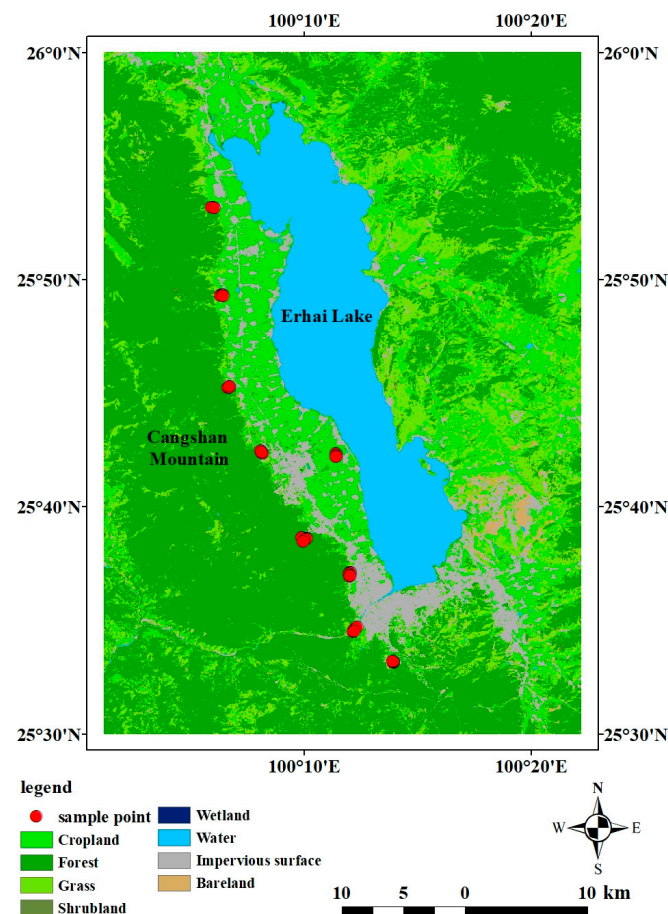| Sample Plot Number	Longitude	Latitude	Land Cover Type
1	100°12′3″ E	25°34′57″ N	Forest
2	100°10′1″ E	25°38′39″ N	Forest
3	100°8′9″ E	25°41′52″ N	Forest
4	100°6′39″ E	25°45′10″ N	Forest
5	100°6′21″ E	25°49′13″ N	Grass
6	100°5′19″ E	25°53′19″ N	Forest
7	100°13′51″ E	25°33′3″ N	Forest
8	100°11′14″ E	25°42′12″ N	Cropland

Figure 2. Location and landcover types of ground sampling sites.

2.2. Methods

The present study utilized a forward simulation dataset from a radiative transfer model to establish look-up tables and investigate the correlation between FMC and vegetation

index/water index, with the aim of developing an expedited FMC estimation model. The overall procedure of this study is illustrated in Figure 3.
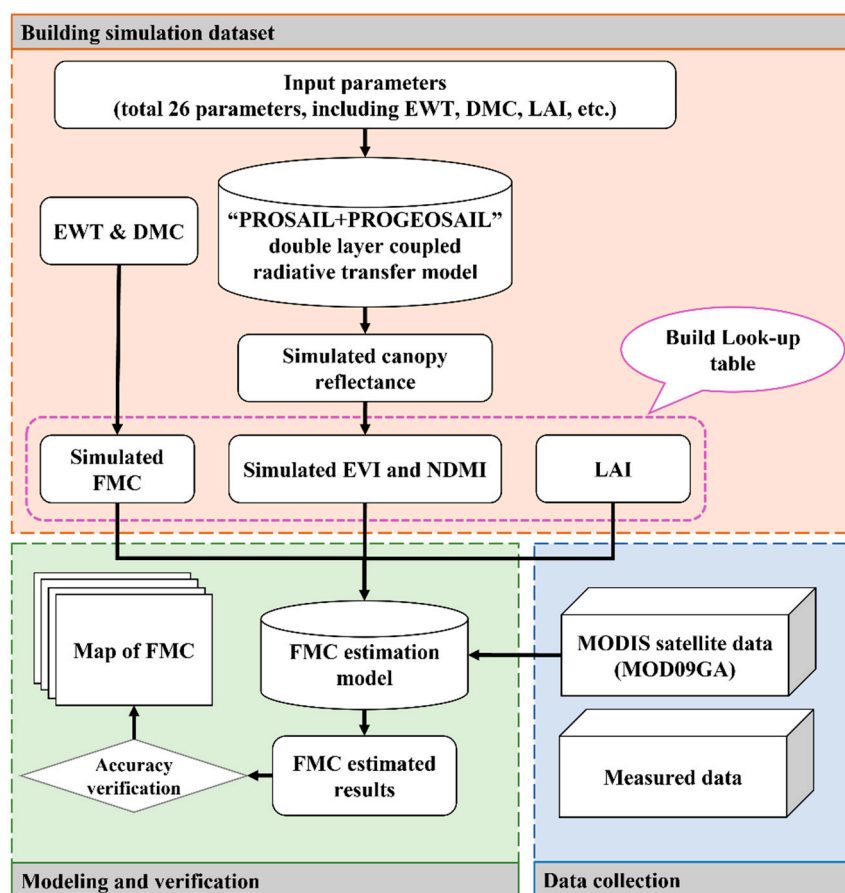
Figure 3. Flowchart of this study.

2.2.1. Radiative Transfer Model

In this study, a two-layer coupled model based on PROSAIL and PROGEOSAIL was employed to simulate the vegetation structural characteristics of "tall trees + low vegetation" in the study area. The PROSAIL model is a mathematical model utilized for simulating the spectral characteristics of vegetation, commonly employed in remote sensing and vegetation monitoring research. Grounded on photosynthesis principles, the PROSAIL model incorporates factors such as leaf structure, light transmission, and reflection to enable the simulation of the spectral response of diverse vegetation types within the visible and near-infrared bands. The PROGEOSAIL model is based on PROSAIL and incorporates a geometric optical model to accurately depict the reflectance of non-continuous canopies.

In this two-layer coupled model, the PROSAIL model was used to simulate the spectral reflectance of the lower grass layer, while the PROGEOSAIL model was utilized to estimate the canopy spectral reflectance of the upper tree layer. The coupling of these models was achieved by replacing the soil reflectance in the PROGEOSAIL model with the spectral reflectance of the lower grassland simulated by the PROSAIL model [22]. This model requires a total of 27 input parameters, including 12 parameters for the lower model and 15 parameters for the upper model. All parameters used in this model are listed in Table 3.

Table 3. The PROSAIL + PROGEOSAIL model input parameters.

Model	Input Parameter	Symbol	Unit	Value
PROSPECT (Lower plants)	Leaf structural parameters	N	/	2
	Chlorophyll content	C_{ab}	$\mu g \cdot cm^{-2}$	40
	Carotenoid content	C_{ar}	$\mu g \cdot cm^{-2}$	8
	Brown pigment fraction	C_{brown}	/	0
	Equivalent water thickness	EWT	$g \cdot cm^{-2}$	0.015
	Dry matter weight	DMC	$g \cdot cm^{-2}$	0.008
SAIL (Lower plants)	Solar zenith angle	tts	(°)	30
	Observed zenith angle	tto	(°)	0
	Leaf area index	LAI	/	2
	Leaf inclination distribution function	LIDFa	/	−0.35
		LIDFb	/	−0.15
	Hot spot effect factor	hspot	/	0.02
	Soil reflectance	Rsoil	/	0.47
PROSPECT (Upper forest)	Leaf structural parameters	N	/	2
	Chlorophyll content	C_{ab}	$\mu g \cdot cm^{-2}$	40
	Carotenoid content	C_{ar}	$\mu g \cdot cm^{-2}$	8
	Brown pigment fraction	C_{brown}	/	0
	Equivalent water thickness	EWT	$g \cdot cm^{-2}$	0.005–0.02
	Dry matter weight	DMC	$g \cdot cm^{-2}$	0.001–0.015
GEOSAIL (Upper forest)	Solar zenith angle	tts	(°)	30
	Observed zenith angle	tto	(°)	0
	Leaf area index	LAI	/	0–6
	Leaf inclination distribution function	LIDFa	/	−0.35
		LIDFb	/	−0.15
	Canopy cover	Ccover	/	0.85
	Canopy height-to-width ratio	CHW	/	2
	Crown shape	/	/	Cone
	Hot spot effect factor	hspot	/	0.02
	Soil reflectance	Rsoil	/	Lower plants' reflectance

2.2.2. Sensitivity Analysis

In the two-layer coupled model, these parameters exhibited varying degrees and ranges of influence within the 400–2500 nm band. This study assumed that each input parameter in the model independently affects the simulation results and conducted a sensitivity analysis on each parameter of the upper-model input. The Car parameter was fixed at 8 $\mu g \cdot cm^{-2}$, Cbrown was fixed at 0 $\mu g \cdot cm^{-2}$, and the observed geometric parameters tts and tto were fixed at 30° and 0°, respectively. The leaf inclination distribution function (LIDF) was assumed to have a spherical distribution, and the crown shape was fixed at cone. The other parameters requiring testing in the sensitivity analysis were set to the values specified in Table 4.

Table 4. Base values used for model test parameters of sensitivity analysis.

Input Parameter	Symbol	Unit	Base Value
Leaf structural parameters	N	/	2
Chlorophyll content	Cab	$\mu g \cdot cm^{-2}$	40
Carotenoid content	Car	$\mu g \cdot cm^{-2}$	8
Brown pigment fraction	Cbrown	/	0
Equivalent water thickness	EWT	$g \cdot cm^{-2}$	0.015
Dry matter weight	DMC	$g \cdot cm^{-2}$	0.008
Solar zenith angle	tts	(°)	30
Observed zenith angle	tto	(°)	0
Leaf area index	LAI	/	2
Leaf inclination distribution function	LIDFa	/	−0.35
	LIDFb	/	−0.15
Hot spot effect factor	hspot	/	0.02
Soil reflectance	Rsoil	/	0.47

2.2.3. Construction of Total Look-Up Table

When employing the physical model for forward simulation of FMC, it is crucial to emphasize the influence of four input parameters, i.e., leaf structural parameters (N), leaf water content (EWT), dry matter content (DMC), and leaf area index (LAI), on the spectral reflectance profile within the 800–2000 nm band. Given the extensive input parameters required by the double-layer coupled model, it is imperative to further streamline variation parameters and simplify the model based on the specific conditions in the study area. This approach will help mitigate potential issues related to the pathological retrieval of the model. In this study, the N value was set as a constant based on the stable vegetation growth conditions in the mountainous forest study area. EWT, DMC, and LAI were considered variable parameters in the upper model, while the other parameters remained fixed during the forward simulation. All model parameters were defined as shown in Table 2 from established references and previous experience. Specifically, the EWT values were selected within the range of 0.005–0.02 with an increment of 0.001, the DMC values ranged from 0.001 to 0.015 with an increment of 0.001, and the LAI values ranged from 0 to 6 with an increment of 0.1.

As the model simulated hyperspectral data with a resolution of 1 nm and the MODIS data image provided wide-band reflectance information, it was necessary to convert the simulated hyperspectral data into wide-band data through spectral equivalence calculation [32]. The equivalence formula is

$$\rho_{multi}(\lambda i) = \frac{\sum \rho(\lambda) f(\lambda i)}{f(\lambda i)} \tag{2}$$

where $\rho_{multi}(\lambda_i)$ is the reflectance of the channel with wavelength, λ_i is the wavelength, $\rho(\lambda)$ is the hyperspectral reflectance, and $f(\lambda_i)$ is the spectral response function of the channel at wavelength λ_i in the multispectral data center. The wavelength ranges of the MODIS 01, 02, 03, and 07 band reflectance data were obtained through equivalent calculation. We further calculated the simulated enhanced vegetation index (EVI), the normalized differential water moisture index (NDMI), and the FMC and constructed a look-up table comprising EWT, DMC, LAI, and FMC. In particular, EVI and NDMI are calculated as

$$EVI = 2.5 \times \frac{\rho_{NIR} - \rho_{RED}}{\rho_{NIR} + 6 \times \rho_{RED} - 7.5 \times \rho_{BLUE} + 1} \tag{3}$$

$$NDMI = \frac{\rho_{NIR} - \rho_{SWIR}}{\rho_{NIR} + \rho_{SWIR}} \tag{4}$$

where ρ_{BLUE} is MODIS data band 01, ρ_{RED} is MODIS data band 02, ρ_{NIR} is MODIS data band 03, and ρ_{SWIR} is MODIS data band 07. In the upper model, PROGeoSAIL, the FMC estimate formula is [33,34]

$$FMC = \frac{EWT}{DMC} \times 100\% \tag{5}$$

2.2.4. Correlation Analysis

In constructing the total look-up table, the combined influence of EVI, NDMI, and LAI on FMC can introduce ambiguity into the overall relationship between the independent variables and the dependent variable. To address this issue, a method was employed whereby LAI was temporarily held at a fixed value. Consequently, several sub-look-up tables containing only two variables, EVI and NDMI, were constructed. These sub-look-up tables were subsets derived from the total look-up table. By visually representing the total look-up table and the sub-look-up tables separately by using scatter plots, it can be observed that when LAI is fixed, the scatter distribution within each sub-look-up table exhibits a regular surface-like pattern. Moreover, the scatter distribution of the total look-up table can be seen as a combination of the scatter surfaces from the various sub-look-up tables. This suggests that there exists an identifiable mathematical pattern among FMC,

EVI, and NDMI when LAI remains constant. The scatter plots depicted in Figure 4 visually demonstrate the aforementioned findings.
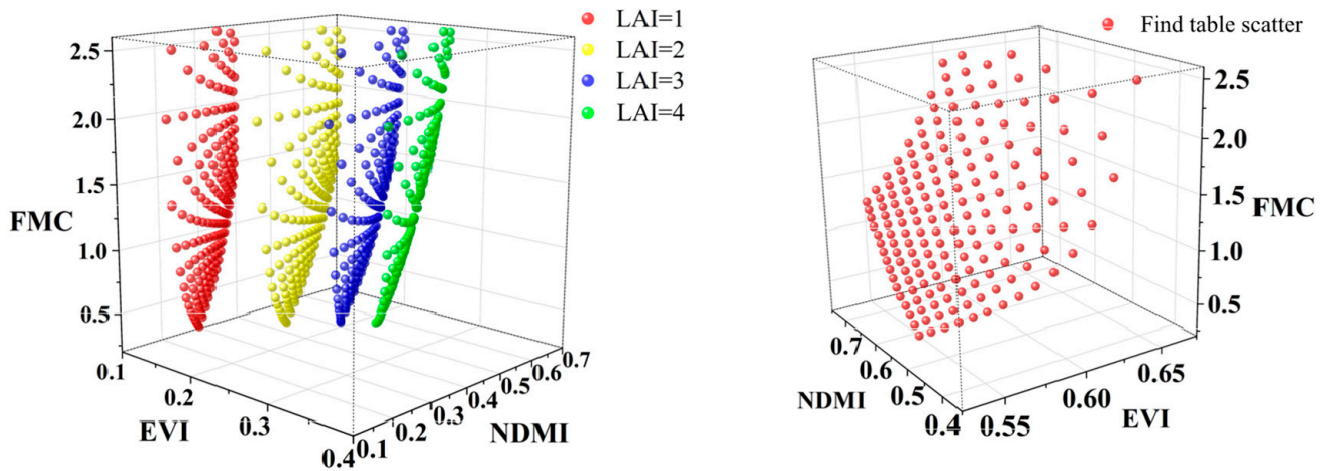

Figure 4. Scatter plots for total and sub-look-up tables.

The correlation between EWT, DMC, and the simulated EVI and NDMI in the sub-look-up table was further investigated in conjunction with Equation (5). It was found that when LAI is held constant as a precondition, there exists an approximate quadratic relationship between EVI and FMC for a fixed value of EWT. Similarly, there exists an approximate linear relationship between NDMI and FMC for a fixed value of DMC. These functional relationships become more pronounced as the LAI values increase. This finding may also account for the regular surface observed in the scatter plot of the sub-look-up table when LAI is fixed.

Based on the observations derived from the sub-look-up table, there is a binary-quadratic functional relationship among EVI, NDMI, and FMC. By integrating Equation (5) with the established correlations between EWT and EVI, as well as between DMC and NDMI, an estimation model can be constructed [35,36].

2.2.5. Estimation of FMC

Based on the aforementioned analysis, considering LAI as a predetermined constant, a quadratic function is employed with EVI as the independent variable to characterize EWT. Similarly, a primary function is utilized with NDMI as the independent variable to characterize DMC. By incorporating both functions into Equation (5), an FMC estimation model is constructed with EVI and NDMI serving as input parameters:

$$\text{FMC} = \frac{a_1 x^2 + a_2 x + a_3}{a_4 y + a_5} \tag{6}$$

where x is the value of EVI, y is the value of NDMI, and a_1–a_5 are the coefficients of the model for the case where LAI is a fixed value. The model coefficients a_1–a_5 were determined through the least square method and integrated to obtain the model parameter matrix for the entire look-up table, which comprises several sub-look-up tables.

Based on the parameter matrix figures and the scatter plot of the total look-up table, it is evident that an increase in LAI results in a growing overlap in the independent variable thresholds of neighboring surfaces. This is visually represented in Figure 5 by the decreasing distance between neighboring surfaces in the scatter plot. Consequently, estimating FMC based solely on these overlapping thresholds can lead to overestimated or underestimated values, or even multiple possible results. To address this issue, it is necessary to correct the step size of the LAI parameter. Previous research has demonstrated that setting parameter step sizes according to a normal distribution can enhance estimation

accuracy when using models like PROSAIL for vegetation physical parameter inversion [37]. Therefore, during actual calculations, the coefficient matrix should be constructed by selecting a set of predetermined values within the LAI value range.
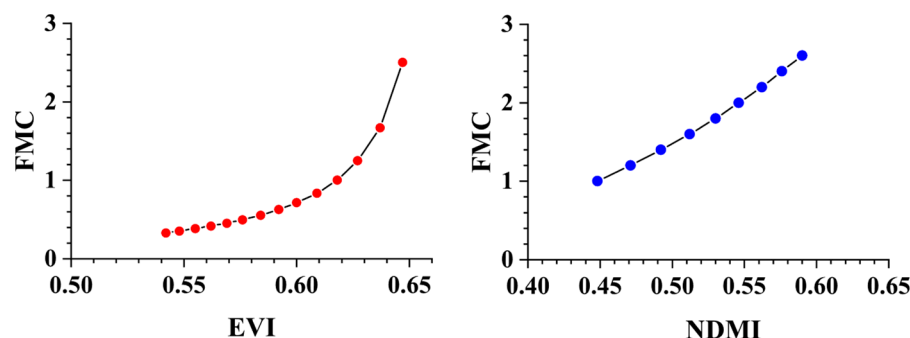

Figure 5. Relationship between EVI/NDMI and FMC (LAI = 3; EWT and DMC = 0.005).

3. Results

3.1. Results of Sensitivity Analysis

The influence of the change in each input parameter on the spectral curve is shown in Figure 6. The above analysis demonstrates that FMC exhibits sensitivity in both the NIR and SWIR bands. According to the analysis, Figure 6a–g show the spectral response of the model output reflectance to the seven model input parameters. Figure 6a shows that the leaf structure parameter (N) affects reflectance throughout the 400–2500 nm band range, with the reflectance increasing as N increases. Figure 6b shows that the chlorophyll content (Cab) mainly affects reflectance in the 400–800 nm band, with the reflectance decreasing as Cab increases. Figure 6c shows that the equivalent water thickness (EWT) has an effect on reflectance in the 1000–2500 nm band, with the reflectance decreasing as EWT increases. At 1450 nm and 1650 nm, EWT has the most significant effect on reflectance and has the greatest effect on reflectance near 1650 nm. Figure 6d shows that leaf dry matter content (DMC) has an effect on reflectance in the 800–2500 nm band, with the reflectance decreasing as DMC increases. Figure 6e shows that leaf area index (LAI) has a significant effect on reflectance throughout the 400–2500 nm band. In the 700–1100 nm range, the reflectance increases with the increase in LAI, but in the 500–700 nm and 1800–2500 nm ranges, the reflectance decreases with the increase in LAI. In particular, the effect of LAI on canopy reflectance is the most pronounced around 700–1450 nm and 1650 nm [38]. Figure 6f,g show that canopy height-to-width ratio (CHW) and canopy cover (Ccover) have little or no effect on reflectance across the 400–2500 nm band.

3.2. Model Coefficient Matrix

In this research, a set of 26 representative LAI values were selected: 0.1, 0.12, 0.14, 0.16, 0.18, 0.2, 0.23, 0.26, 0.3, 0.35, 0.4, 0.45, 0.5, 0.55, 0.6, 0.7, 0.8, 0.9, 1.1, 1.3, 1.6, 2.1, 2.6, 3.0, 4.0, and 6.0. The selection of LAI values was based on the consideration that the range of independent variables in these surfaces covers the entire range of EVI while minimizing overlap between adjacent surfaces' independent variable ranges as much as possible. For unselected surfaces corresponding to other fixed LAI values, using these 26 selected surfaces can fully compensate for their calculation, since their EVI and NDMI value ranges overlap completely with those of the selected surfaces, and the distances between them are very close. This approach helps reduce the size of the parameter matrix and simplifies the overall model. Table 5 shows the LAI values and the corresponding fitting coefficients for 26 representative surfaces.
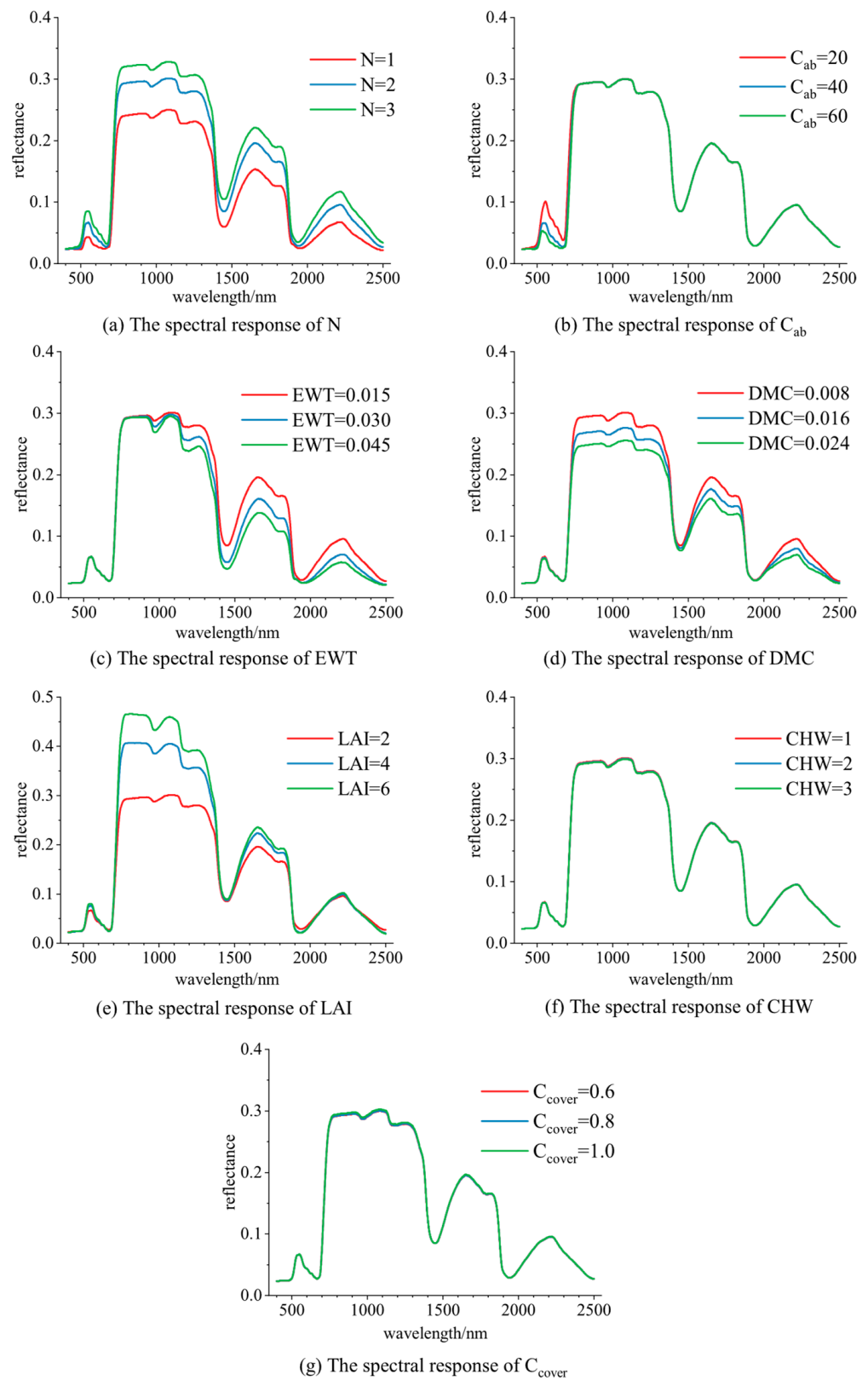
(a) The spectral response of N

(b) The spectral response of C_{ab}

(c) The spectral response of EWT

(d) The spectral response of DMC

(e) The spectral response of LAI

(f) The spectral response of CHW

(g) The spectral response of C_{cover}

Figure 6. The results of the parameter sensitivity analysis.

Table 5. Simplified model parameter matrix for FMC estimation, where a_1 to a_5 are the empirical parameters in Equation (6).

LAI	a_1	a_2	a_3	a_4	a_5
0.1	3069.379	−846.395	58.362	−0.634	0.154
0.12	996.128	−285.384	20.446	−0.219	0.057
0.14	1587.222	−470.94	34.943	−0.401	0.109
0.16	1365.025	−418.881	32.146	−0.435	0.124
0.18	1104.593	−349.556	27.667	−0.412	0.123
0.2	1073.114	−351.119	28.733	−0.377	0.118
0.23	1063.039	−363.702	31.124	−0.43	0.142
0.26	946.679	−337.517	30.102	−0.446	0.156
0.3	831.378	−312.011	29.293	−0.465	0.171
0.35	668.267	−266.844	26.66	−0.42	0.167
0.4	695.166	−293.326	30.97	−0.513	0.214
0.45	553.187	−245.027	27.162	−0.517	0.226
0.5	449.88	−208.998	24.301	−0.474	0.217
0.55	459.904	−223.352	27.153	−0.538	0.257
0.6	358.562	−181.497	22.999	−0.468	0.230
0.7	350.395	−190.789	26.013	−0.593	0.309
0.8	359.677	−209.316	30.509	−0.739	0.403
0.9	266.166	−164.52	25.473	−0.634	0.36
1.1	246.09	−168.358	28.862	−0.802	0.484
1.3	218.468	−162.609	30.342	−0.926	0.588
1.6	158.4	−130.511	26.976	−0.973	0.652
2.1	15.362	−14.354	3.369	−0.156	0.111
2.6	13.508	−13.804	3.584	−0.209	0.154
3.0	14.264	−15.376	4.175	−0.297	0.224
4.0	2.726	−3.213	0.958	−0.104	0.081
6.0	3.074	−3.91	1.271	−0.268	0.213

3.3. Mapping of FMC

According to the calibrated model, MODIS data were utilized for estimating the local FMC within the study area on 24 March 2023. This facilitated the subsequent accuracy verification by enabling a convenient comparison between the estimated results and the measured data. Figure 7 shows the FMC estimation results for the study area. We can observe that the FMC in the study area in March was generally low, which is consistent with the higher occurrence of wildfires during the local dry season.
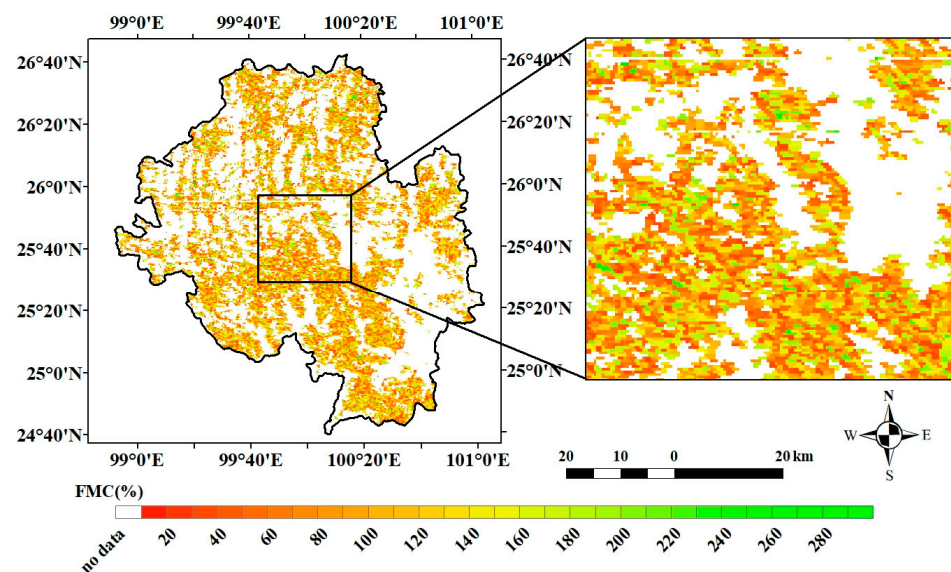
Figure 7. Map of FMC estimation results for study area (date: 24 March 2023).

3.4. Validation of Measured Data

The calculated results of the model were compared with the actual measured data for eight corresponding pixels, as depicted in Figure 8. The blue dots are plotted with estimated and actual measured values as horizontal and vertical coordinates, and the orange lines fitted from these points. It is evident that the overall estimation outcomes exhibit closer proximity to the actual measurements, with a coefficient of determination (R2) reaching 0.79. Based on the FMC estimation results across the entire study area, it can be observed that the overall FMC values are slightly lower than those found in normal forests, predominantly ranging between 60% and 120%. This confirms that the FMC estimated from MODIS data aligns well with ground-truth conditions. Since 2023, Yunnan Province has experienced a prolonged period of dry weather, resulting in frequent forest fires. During data collection in the study area, local forest fire danger warnings remained active, contributing to the lower local FMC values. Both the FMC from ground measurements and remote sensing retrieval effectively support this phenomenon.
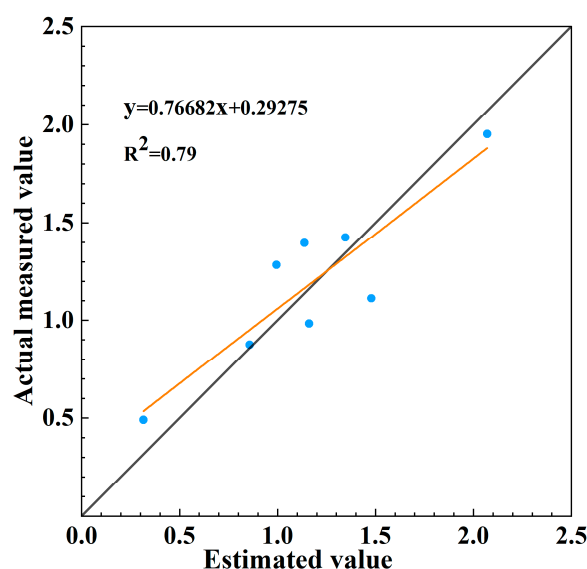

Figure 8. Comparison between the FMC from ground measurements and remote sensing retrieval at the sampling sites.

3.5. Applicability Test of the FMC Estimation Method

To further validate the reliability of the estimation model, this study selected several historical fire events to estimate the pre-disaster FMC in the affected area and generated corresponding maps [39]. Due to significant cloud cover in Yunnan during early April 2023, some surface reflectance data were missing. Consequently, the forest fire event that occurred on 19 August 2022 in Chongqing was chosen for investigation. MODIS data from 12–18 August 2022 were employed to estimate the FMC in the Chongqing area before the fire. As shown in Figure 9, a declining trend in overall FMC levels within Chongqing during the week preceding the fire incident can be observed. Moreover, consistently low FMC values were observed specifically in the western Chongqing region, which was an area where initial fires ignited during this event. This trend indicates that FMC as an indicator has a certain representativeness in forest fire risk assessment and also indirectly indicates the accuracy and universality of the FMC estimation method proposed in this study [40].
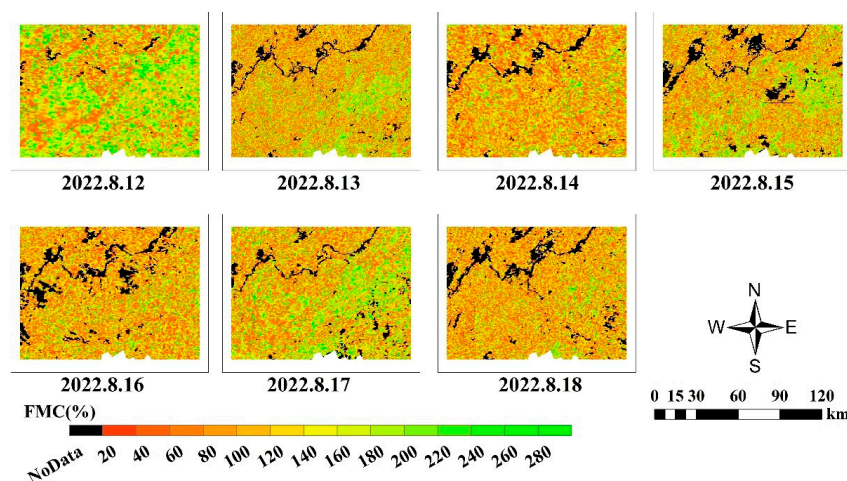
Figure 9. FMC estimation results for the week before the 8.19 fire in the algorithm verification area in 2022.

4. Discussion

4.1. Comparison of FMC Estimation Models

In this study, a correlation between FMC and the vegetation index/water index was identified through physical modeling. This finding is consistent with the conclusions drawn by other scholars who have investigated the relationship between the vegetation index and FMC using different physical models [41]. In further developing the estimation model for vegetation index, water index, and FMC, it was observed that a single vegetation index or water index exhibited limited correlation with FMC. However, by increasing the number of independent variables and using the combination of vegetation index and water index to construct the FMC estimation model, a strong correlation among these variables was effectively expressed. The proposed method exhibits similar accuracy to the empirical model while mitigating the limitations of the empirical model itself.

When utilizing physical models for inverting target vegetation parameters, many scholars have employed look-up tables to simulate the target parameters in a forward direction and utilized a loss function to approximate the inverted object within the look-up table, which has been proven to be highly accurate [42]. However, the loss function always presents a certain amount of error, and the look-up table itself does not adequately represent the relationship between the input parameters and the target system parameters in the model. Establishing a direct regression equation between input parameters and target parameters enables a more explicit reflection of their relationship while circumventing errors introduced by the loss function. Although the model itself may contain some errors, compared with using look-up tables combined with loss functions, the errors are reduced [43]. With further investigation into the correlation between vegetation index/water index and FMC, improvements can be made to enhance both functional aspects used in establishing such models, as well as the accuracy levels of FMC estimation models.

4.2. Impact Factor of the Model

4.2.1. Robustness Analysis

The estimation results of this model are primarily influenced by the input parameters EVI and NDMI. To assess the model's robustness, error was deliberately introduced in these parameters. The findings reveal that when both EVI and NDMI were incrementally increased from 0.02 to 0.2 with an interval of 0.02, the error in estimating FMC using the model remained consistently within the range of -270% to 250%. These results provide evidence supporting the robustness of the estimation model to some extent.

4.2.2. Effect of LAI

The study demonstrates that the variation in LAI significantly impacts the spectral reflectance of vegetation within the 800–2000 nm band, and several bands within this range are sensitive to vegetation water content. This result indicates that the value of LAI has an impact on this model [44,45]. In our study, we observed a decrease in correlation between vegetation index/water index and FMC when the LAI values were low. This is evident in the scatter plot, where the surface of the corresponding sub-look-up table becomes irregular and less smooth with lower LAI values. Consequently, fitting coefficients to sub-look-up tables with lower LAI values yields larger coefficient values. This partially compromises the stability of the model during its application. However, since our research focuses on forest canopies within an LAI range typically falling between 1 and 3, all sub-look-up tables within this range display clear regularity. As a result, fitting yields significantly reduced model coefficients. Therefore, in practice, smaller model coefficients are typically employed for most FMC calculations, alleviating some of the model's instability.

4.3. Indicator Potential of FMC for Forest Fires

As one of the indicators reflecting the moisture level of forests, the trend of fuel moisture content (FMC) can, to some extent, indicate forest fire risk. This conclusion has been validated through application tests involving forest fire incidents, and other researchers have reached similar conclusions when conducting FMC inversion and forest fire-related studies by using different methods [5,46]. However, in practical applications, it is more scientifically sound to evaluate the overall environment of the forest from multiple perspectives, including climate, topography, vegetation, and so on, based on the principle of forest fire prediction [47,48]. FMC is not the sole determining factor in the occurrence of forest fires, but it is undoubtedly representative among these various influencing factors.

4.4. Limitations and Future Research

4.4.1. Effect of Terrain

Although the PROSAIL + PROGeoSAIL model does not need to consider the influence of terrain and vegetation type, the study area's high altitude and drastic topographic relief inevitably affected the accuracy of the model to some extent [49,50]. Additionally, shadows caused by mountain fluctuations may introduce certain challenges to the model. While previous studies have suggested that estimating FMC by using EVI can partially alleviate issues related to mountain shading, this paper did not investigate the impact of mountain shadows on the model or assess how much mitigation is achieved after employing EVI. These factors were not considered in this study and may lead to errors in the estimation model due to topographic factors.

4.4.2. Cloud Interference

Cloudy weather conditions in the study area had an impact on this research. The frequent occurrence of thick cloud cover often resulted in missing optical data used for analysis, which posed challenges in monitoring long-term changes in FMC within the local forested area [51,52].

4.4.3. Limitation of Model Validation

Due to the complex terrain in the research area and limited field measurement time, the number of sample points collected for model accuracy verification is relatively small. Additionally, considering the specific requirements of long-term FMC monitoring for remote sensing data temporal resolution, this study opted for MODIS reflectance data with a spatial resolution of 500 m after careful consideration, sacrificing some spatial accuracy while ensuring daily temporal resolution. In future studies, it is essential to acquire more field measurement data and employ satellite images with higher precision, such as Landsat, to further validate the proposed model's accuracy.

4.4.4. Future Research

In subsequent studies, we will further analyze a range of effects resulting from mountainous terrain relief and weather conditions. These factors will be considered when optimizing the model to mitigate the modeling errors caused by terrain problems. To validate the model's applicability on high-precision images, additional field data collection experiments will be conducted in subsequent research. The accuracy and reliability of the proposed model may be further validated and substantiated through the utilization of high-resolution satellite imagery such as Landsat [53].

5. Conclusions

In this study, an FMC estimation method based on the combination of EVI and NDMI was introduced. This method provided estimates of FMC, taking into account the correlation between EVI/NDMI and FMC. The accuracy of the proposed method was validated by using field measurement data. Additionally, the model was applied to estimate FMC in the week leading up to the forest fire that occurred in Chongqing in August 2022. The study yielded the following key findings:

(1) Leaf structural parameter (N), equivalent water thickness (EWT), dry matter weight (DMC), and leaf area index (LAI) exhibited significant influence on the spectral curves generated by the two-layer coupled model employed for forward simulation. Notably, LAI had a strong impact on the 700–1450 nm and 1650 nm bands, which are particularly sensitive to vegetation water content. Consequently, it was observed that variations in LAI played a crucial role in achieving an accurate estimation of FMC.

(2) A distinct correlation was observed when combining the vegetation index, water index, and FMC. An estimation method based on a combination of EVI–NDMI was developed to directly calculate FMC. Compared with the traditional FMC estimation model, this method eliminated errors arising from using the loss function in physical model-based forward simulations.

(3) Using the estimation model, the study projected the FMC one week before the Chongqing forest fire in 2022 and identified a significant declining trend in the local FMC leading up to the fire event. This trend highlights the effectiveness of early forest fire warnings made possible by the proposed FMC estimation model.

References

1. Szpakowski, D.; Jensen, J. A Review of the Applications of Remote Sensing in Fire Ecology. *Remote Sens.* **2019**, *11*, 2638. [CrossRef]
2. Tian, X.; Shu, L. Forest Fires and Sustainable Development. *World For. Res.* **2003**, *16*, 38–41. [CrossRef]
3. Guo, F.; Zhang, L.; Jin, S.; Tigabu, M.; Su, Z.; Wang, W. Modeling Anthropogenic Fire Occurrence in the Boreal Forest of China Using Logistic Regression and Random Forests. *Forests* **2016**, *7*, 250. [CrossRef]
4. Pyne, S.J. *Introduction to Wildland Fire. Fire Management in the United States*; John Wiley & Sons: Hoboken, NJ, USA, 1984.

5. Gale, M.G.; Cary, G.J.; Van Dijk, A.I.J.M.; Yebra, M. Forest fire fuel through the lens of remote sensing: Review of approaches, challenges and future directions in the remote sensing of biotic determinants of fire behaviour. *Remote Sens. Environ.* **2021**, *255*, 112282. [CrossRef]

6. Arcos, M.A.; Balaguer-Beser, Á.; Ruiz, L.Á. Live fuel moisture content modeling and mapping using spectral, meteorological, and topographic data. In Proceedings of the Ninth International Conference on Remote Sensing and Geoinformation of the Environment (RSCy2023), Ayia Napa, Cyprus, 3–5 April 2023; pp. 21–29. [CrossRef]

7. Hyoung, L.J. Prediction of Large-Scale Wildfires With the Canopy Stress Index Derived from Soil Moisture Active Passive. *Ieee J. Sel. Top. Appl. Earth Obs. Remote Sens.* **2021**, *14*, 2096–2102. [CrossRef]

8. Przezdziecki, K.; Zawadzki, J.; Cieszewski, C.; Bettinger, P. Estimation of soil moisture across broad landscapes of Georgia and South Carolina using the triangle method applied to MODIS satellite imagery. *Silva Fenn.* **2017**, *51*, 1683. [CrossRef]

9. Luo, K.; Quan, X.; He, B.; Yebra, M. Effects of Live Fuel Moisture Content on Wildfire Occurrence in Fire-Prone Regions over Southwest China. *Forests* **2019**, *10*, 887. [CrossRef]

10. Cawson, J.G.; Duff, T.J.; Tolhurst, K.G.; Baillie, C.C.; Penman, T.D. Fuel moisture in Mountain Ash forests with contrasting fire histories. *For. Ecol. Manag.* **2017**, *400*, 568–577. [CrossRef]

11. Li, M.; Jiao, M.; Wang, W.; Chen, R.; Fan, C. Global Live Fuel Moisture Content Dynamic Monitoring Based on Modis Data Observation. In Proceedings of the IGARSS 2023—2023 IEEE International Geoscience and Remote Sensing Symposium, Pasadena, CA, USA, 16–21 July 2023; pp. 3303–3306. [CrossRef]

12. Leblon, B. Monitoring forest fire danger with remote sensing. *Nat. Hazards* **2005**, *35*, 343–359. [CrossRef]

13. Saatchi, S.; Halligan, K.; Despain, D.G.; Crabtree, R.L. Estimation of forest fuel load from radar remote sensing. *IEEE Trans. Geosci. Remote Sens.* **2007**, *45*, 1726–1740. [CrossRef]

14. Deng, B.; Yang, W.N.; Mu, N.; Zhang, C. The Research of Vegetation Water Content Based on Spectrum Analysis and Angle Slope Index. *Spectrosc. Spectr. Anal.* **2016**, *36*, 2546–2552.

15. Tang, Y.; Wang, X.; Lu, C.; Zhao, C. Estimating the canopy water content of alfalfa based on the PROSAIL model and spectral index. *J. Lanzhou Univ. Nat. Sci.* **2023**, *59*, 55–62. [CrossRef]

16. Jacquemoud, S.; Baret, F. PROSPECT: A model of leaf optical properties spectra. *Remote Sens. Environ.* **1990**, *34*, 75–91. [CrossRef]

17. Kötz, B.; Schaepman, M.; Morsdorf, F.; Bowyer, P.; Itten, K.; Allgöwer, B. Radiative transfer modeling within a heterogeneous canopy for estimation of forest fire fuel properties. *Remote Sens. Environ.* **2004**, *92*, 332–344. [CrossRef]

18. Jacquemoud, S. Inversion of the PROSPECT + SAIL canopy reflectance model from AVIRIS equivalent spectra: Theoretical study. *Remote Sens. Environ.* **1993**, *44*, 281–292. [CrossRef]

19. Dawson, T.P.; Curran, P.J.; Plummer, S.E. LIBERTY—Modeling the effects of leaf biochemical concentration on reflectance spectra. *Remote Sens. Environ.* **1998**, *65*, 50–60. [CrossRef]

20. Huemmrich, K.F. The GeoSail model: A simple addition to the SAIL model to describe discontinuous canopy reflectance. *Remote Sens. Environ.* **2001**, *75*, 423–431. [CrossRef]

21. Gastelluetchegorry, J.P.; Pinel, V.; Zagolski, F.; Demarez, V. Modeling radiative transfer in heterogeneous 3D vegetation canopies. In Proceedings of the Conference on Multispectral and Microwave Sensing of Forestry, Hydrology, and Natural Resources, Rome, Italy, 26–30 September 1994; pp. 38–49. [CrossRef]

22. Xie, Q.; Quan, X.; He, B. Wildfire Danger Assessment Over Southwest China Based on Short-Term Features of Weather and Fuel Variables. In Proceedings of the 2021 IEEE International Geoscience and Remote Sensing Symposium, IGARSS 2021, Brussels, Belgium, 12–16 July 2021; pp. 8648–8651. [CrossRef]

23. Yu, Y.; Fan, W.; Yang, X. Comparisons of three models for vegetation canopy bi-directional reflectance distribution function. *Acta Phytoecol. Sin.* **2012**, *36*, 55–62. [CrossRef]

24. Marino, E.; Yebra, M.; Guillén-Climent, M.; Algeet, N.; Tomé, J.L.; Madrigal, J.; Guijarro, M.; Hernando, C.J.R.S. Investigating live fuel moisture content estimation in fire-prone shrubland from remote sensing using empirical modelling and RTM simulations. *Remote Sens.* **2020**, *12*, 2251. [CrossRef]

25. Wang, L.; Hunt, E.R.; Qu, J.J.; Hao, X.; Daughtry, C.S.T. Remote sensing of fuel moisture content from ratios of narrow-band vegetation water and dry-matter indices. *Remote Sens. Environ.* **2013**, *129*, 103–110. [CrossRef]

26. Cunill Camprubí, À.; González-Moreno, P.; Resco de Dios, V.J.R.S. Live fuel moisture content mapping in the Mediterranean Basin using random forests and combining MODIS spectral and thermal data. *Remote Sens.* **2022**, *14*, 3162. [CrossRef]

27. Santos, F.L.M.; Couto, F.T.; Dias, S.S.; Ribeiro, N.d.A.; Salgado, R. Vegetation fuel characterization using machine learning approach over southern Portugal. *Remote Sens. Appl. Soc. Environ.* **2023**, *32*, 101017. [CrossRef]

28. Cao, Y.; Wang, M.; Liu, K. Wildfire Susceptibility Assessment in Southern China: A Comparison of Multiple Methods. *Int. J. Disaster Risk Sci.* **2017**, *8*, 164–181. [CrossRef]

29. Lai, G.K.; Quan, X.W.; He, B.B. Assessment of the Effect of PROSAILH for Open and Closed Shrublands Live Fuel Moisture Content Retrieval. In Proceedings of the IEEE International Geoscience and Remote Sensing Symposium (IGARSS), Electr Network, Waikoloa, HI, USA, 26 September–2 October 2020; pp. 6778–6781. [CrossRef]

30. Li, H.; Fan, W.; Yu, Y.; Yang, X. Leaf Area Index Retrieval Based on Prospect, Liberty and Geosail Models. *Sci. Silvae Sin.* **2011**, *47*, 75–81. [CrossRef]

31. Quan, X.; He, B.; Liu, X.; Liao, Z.; Qiu, S.; Yin, C. Retrieval of fuel moisture content by using radiative transfer models from optical remote sensing data. *J. Remote Sens.* **2019**, *23*, 62–77. [CrossRef]

32. Mo, Y.; Zhang, W.; Zhang, L. Simulation of Hyperspectral Remote Sensing Image Based on PROSAIL Model. *Infrared* **2016**, *37*, 1–7.
33. Quan, X.; Li, Y.; He, B.; Cary, G.J.; Lai, G. Application of Landsat ETM+ and OLI Data for Foliage Fuel Load Monitoring Using Radiative Transfer Model and Machine Learning Method. *IEEE J. Sel. Top. Appl. Earth Obs. Remote Sens.* **2021**, *14*, 5100–5110. [CrossRef]
34. Quan, X.; Xie, Q.; He, B.; Luo, K.; Liu, X. Integrating remotely sensed fuel variables into wildfire danger assessment for China. *Int. J. Wildland Fire* **2021**, *30*, 822. [CrossRef]
35. Feng, X.; Zeng, Y.; Wu, Z.; Hang, W.; Wei, S.; Tang, L.; Hu, H. Remote Sensing Retrieval of FMC in Subtropical Forests of Guangdong Based on Satellite Multispectral Data. *J. Univ. Electron. Sci. Technol. China* **2022**, *51*, 432–437.
36. Zhang, X.; Jiao, Z.; Zhao, C.; Yin, S.; Cui, L.; Dong, Y.; Zhang, H.; Guo, J.; Xie, R.; Li, S.; et al. Retrieval of Leaf Area Index by Linking the PROSAIL and Ross-Li BRDF Models Using MODIS BRDF Data. *Remote Sens.* **2021**, *13*, 4911. [CrossRef]
37. Jiang, H.; Chai, L.; Jia, K.; Liu, J.; Yang, S.; Zheng, J. Estimation of water content for short vegetation based on PROSAIL model and vegetation water indices. *J. Remote Sens.* **2021**, *25*, 1025–1036. [CrossRef]
38. Ma, J.; Huang, S.; Li, J.; Li, X.; Song, X.; Leng, P.; Sun, Y. Global Sensitivity Analysis of Parameters in the PROSAIL Model Based on Modified Sobol's Method. *Bull. Surv. Mapp.* **2016**, *3*, 33–35. [CrossRef]
39. Van Hoang, T.; Chou, T.Y.; Fang, Y.M.; Nguyen, N.T.; Nguyen, Q.H.; Xuan Canh, P.; Ngo Bao Toan, D.; Nguyen, X.L.; Meadows, M.E. Mapping Forest Fire Risk and Development of Early Warning System for NW Vietnam Using AHP and MCA/GIS Methods. *Appl. Sci.* **2020**, *10*, 4348. [CrossRef]
40. Caccamo, G.; Chisholm, L.A.; Bradstock, R.A.; Puotinen, M.L. Using remotely-sensed fuel connectivity patterns as a tool for fire danger monitoring. *Geophys. Res. Lett.* **2012**, *39*, 1–5. [CrossRef]
41. Raymond Hunt, E.; Wang, L.; Qu, J.J.; Hao, X. Remote sensing of fuel moisture content from canopy water indices and normalized dry matter index. *J. Appl. Remote Sens.* **2012**, *6*, 061705. [CrossRef]
42. Zhang, J.; Xu, Y.; Yao, F.; Wang, P.; Guo, W.; Li, L.; Yang, L. Advances in estimation methods of vegetation water content based on optical remote sensing techniques. *Sci. China Technol. Sci.* **2010**, *53*, 1159–1167. [CrossRef]
43. Quan, X.; He, B.; Yebra, M.; Yin, C.; Liao, Z.; Li, X. Retrieval of forest fuel moisture content using a coupled radiative transfer model. *Environ. Model. Softw.* **2017**, *95*, 290–302. [CrossRef]
44. Bach, H.; Verhoef, W. Sensitivity studies on the effect of surface soil moisture on canopy reflectance using the radiative transfer model GeoSAIL. In Proceedings of the 23rd International Geoscience and Remote Sensing Symposium (IGARSS 2003), Toulouse, France, 21–25 July 2003; pp. 1679–1681. [CrossRef]
45. Wang, L.; Niu, Z. Sensitivity of Vegetation Parameters based on PROSAIL Model. *Remote Sens. Technol. Appl.* **2014**, *29*, 219–223.
46. Wang, L.; Quan, X.; He, B.; Yebra, M.; Xing, M.; Liu, X. Assessment of the Dual Polarimetric Sentinel-1A Data for Forest Fuel Moisture Content Estimation. *Remote Sens.* **2019**, *11*, 1568. [CrossRef]
47. Costa-Saura, J.M.; Balaguer-Beser, A.; Ruiz, L.A.; Pardo-Pascual, J.E.; Soriano-Sancho, J.L. Empirical Models for Spatio-Temporal Live Fuel Moisture Content Estimation in Mixed Mediterranean Vegetation Areas Using Sentinel-2 Indices and Meteorological Data. *Remote Sens.* **2021**, *13*, 3726. [CrossRef]
48. Wu, X.; Zhang, G.; Yang, Z.G.; Tan, S.Q.; Yang, Y.K.; Pang, Z.H. Machine Learning for Predicting Forest Fire Occurrence in Changsha: An Innovative Investigation into the Introduction of a Forest Fuel Factor. *Remote Sens.* **2023**, *15*, 4208. [CrossRef]
49. Hu, G.; Li, A. BOST: A Canopy Reflectance Model Suitable for Both Continuous and Discontinuous Canopies Over Sloping Terrains. *IEEE Trans. Geosci. Remote Sens.* **2022**, *60*, 4416119. [CrossRef]
50. Hu, H.; Liang, Y.; Sun, L.; Song, Y. Effects of simulated aspect and gradient of slope on moisture of combustible material in laboratory. *J. For. Environ.* **2016**, *36*, 80–85. [CrossRef]
51. He, B.; Liao, Z.; Yin, C.; Quan, X.; Qiu, S.; Xing, M.; Li, X.; Bai, X.; Li, Y.; Xu, D. Theory and application status of quantitative remote sensing in cloudy and hilly regions. *Dianzi Keji Daxue Xuebao/J. Univ. Electron. Sci. Technol. China* **2016**, *45*, 533–550.
52. Wang, W.; Quan, X. Estimation of Live Fuel Moisture Content From Multiple Sources of Remotely Sensed Data. *IEEE Geosci. Remote Sens. Lett.* **2023**, *20*, 3002405. [CrossRef]
53. Hou, X.; Wang, M.; Liu, S.; Gao, S.; Sui, X.; Liang, S.; Wan, H. Comparsion between Prosail Model and Landsat 8 Images in Inversion of Water Content of Wheat Canopy. *J. Triticeae Crops* **2018**, *38*, 493–497.